Research Square

Preprints are preliminary reports that have not undergone peer review.
They should not be considered conclusive, used to inform clinical practice,
or referenced by the media as validated information.

Numerical Investigation for the Cooling Performance of Circular and Rectangular Ground-Coupled Heat Exchangers with Different Geometrical Layouts

Sudhir Kumar

prsudhirk@gmail.com

Maulana Azad National Institute of Technology

Narendra Gajbhiye

Maulana Azad National Institute of Technology

Research Article

Keywords: GCHE, Thermal performance, Friction factor, Air temperature, Reynolds number, Effectiveness

Posted Date: April 9th, 2026

DOI: https://doi.org/10.21203/rs.3.rs-9106831/v1

License: This work is licensed under a Creative Commons Attribution 4.0 International License.
Read Full License

Additional Declarations: No competing interests reported.

"Numerical Investigation for the Cooling Performance of Circular and Rectangular Ground-Coupled Heat Exchangers with Different Geometrical Layouts"

Sudhir Kumar[1], Narendra Gajbhiye[2]

1, Research Scholar, Department of Mechanical Engineering, MANIT, Bhopal, MP-462003

2, Assistant Professor, Department of Mechanical Engineering, MANIT, Bhopal, MP-462003

Corresponding author: Sudhir Kumar

Email: prsudhirk@gmail.com

Abstract

Ground-coupled heat exchangers use geothermal energy storage to provide a sustainable solution for heating, ventilation, and air conditioning. In this study, the performance of circular- and rectangular-cross-section ground-coupled heat exchangers with four layouts (simple horizontal, U-shaped, helical, and slinky) is numerically simulated. It has been found that the rectangular GCHE maintains a more stable air temperature and achieves the maximum temperature drop at a shorter length across all layouts. The temperature at the exit of a circular GCHE with horizontal, U-shaped, helical, and slinky layouts is found to be 302.159 K, 301.586 K, 300.647 K, and 300.20 K, respectively, while the same temperatures are achieved in rectangular GCHEs with corresponding layouts at sections of 18.82 m, 17.46 m, 16.09 m, and 15.43 m, respectively. The length of the slinky layout with a circular cross-section GCHE is reduced by 17%, 13%, and 6% relative to the horizontal, U-shaped, and helical layouts, respectively. In comparison, reductions of 23%, 19%, and 8% are observed for the rectangular cross-section in the corresponding layouts. The inlet velocity significantly impacts the thermal performance of the GCHE, with the maximum temperature reduction occurring at a flow rate of 1 m/s. The average cooling capacity of rectangular cross-sectional GCHE is more than 40% higher than that of circular GCHE for all the layouts studied. The maximum cooling capacity is observed at a higher inlet air temperature of 323 K for a rectangular GCHE with a slinky layout. The friction factor and pressure drop are found to increase with the increase in the Reynolds number. The rectangular GCHEs provides 19.8 % – 40.34% higher cooling capacity compared to circular GCHEs at air velocity increases from 1 m/s to 5 m/s.

Nomenclature

u	Flow rate of air	**Dimensionless parameters**	
A_c	Cross-section of GCHE	Nu	Nusselt number
Cv	Specific heat at constant volume	Re	Reynolds number
D_h	Hydraulic diameter of GCHE	Pr	Prandtl number
m_a	Mass flow rate of air	f	Friction factor
U	Velocity field	E	Effectiveness
L	Length of GCHE		
T	Temperature of air	**Greek letters**	
K	Thermal conductivity of soil	ρ	Air-density
Q_c	Cooling capacity of GCHE	υ	Kinematic viscosity
h	Convective heat transfer coefficient	μ	Dynamic viscosity
Subscripts		μ_t	Turbulent viscosity
ai	Inlet air	ε	Dissipation rate of turbulence
ao	Outlet air		
s	Soil		

Keywords: GCHE, Thermal performance, Friction factor, Air temperature, Reynolds number, Effectiveness

1. Introduction

Thermal and nuclear power plants make major contributions to electricity production, and most countries rely on them. However, the availability of fossil fuels such as coal, natural gas, and petroleum is limited. Energy production through these sources emits environmental pollutants such as CO, NOx, HC, CO_2, and others. These pollutants contribute to global

warming, acid rain, ozone depletion, and natural disasters such as floods and droughts. The production of energy through solar, wind, rain, tides, waves, and geothermal sources is inexhaustible and pollution-free and helps to achieve our energy requirements. The use of solar and wind energy, among other renewable resources, has contributed to an exponential increase. Nowadays, every country wants to reduce its dependency on fossil fuels and try to achieve clean and sustainable energy at a low expenditure. Heating, ventilation, and air conditioning (HVAC) require about one-third of the world's total energy consumption. Conventional HVAC maintains thermal comfort inside the building, requires enormous electrical power, and has numerous environmental issues. The air conditioner produces harmful chemicals such as chlorofluorocarbons (CFCs), nitrogen oxides (NOx), greenhouse gases, etc., to maintain a comfortable temperature inside the buildings. Low energy consumption technology and green technologies are being developed for cooling and comfort conditioning. The buildings may be ventilated utilizing a variety of passive techniques, including solar-wall/solar-chimneys, wind-scoop/wind catcher, evaporative-cooler, cross-venting, ground-coupled heat exchangers, etc. A ground-coupled heat exchanger (GCHE) is one of the effective passive techniques used for building conditioning. At a particular depth of the ground, the temperature variations are found to be almost negligible and observed independent of changes in the ambient conditions. The temperature of the soil beneath the surface is always higher than the ambient temperature in winter and lower in summertime [1,2,3,4,5,6]. The GCHE is installed at a definite depth of the earth's surface and utilizes the stored energy of soil for cooling a building. Figure 1 illustrates the schematic of the GCHE. The GCHE technology would be used alone or in conjunction with other passive/active technologies, such as solar chimneys, solar photovoltaic, solar air heaters, heat pumps, and air conditioning [13,20,21] for the heating and cooling of buildings.

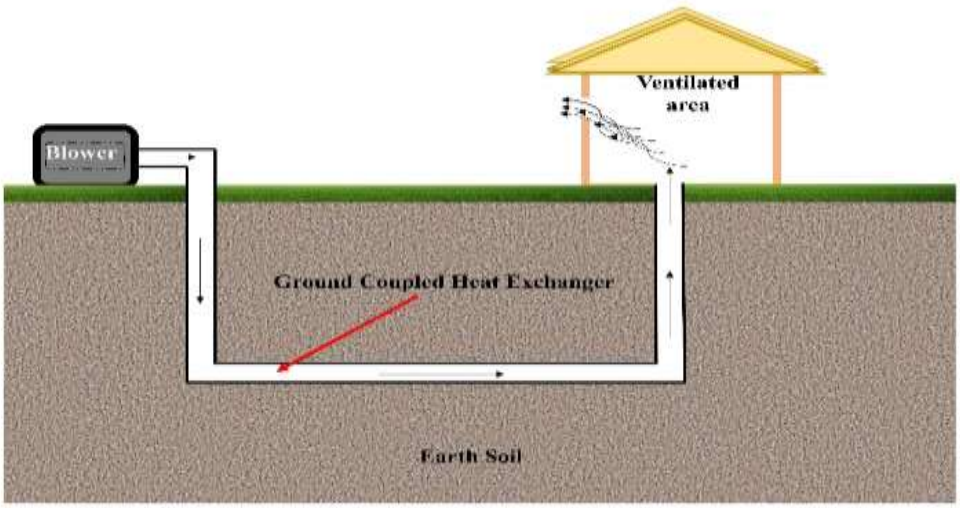


Figure 1. Schematic of GCHE system.

The thermal performance of GCHE was examined under intermittent conditions in the hot and humid environment of Ajmer City, India, by Misra et al. [2]. The study found that soil thermal conductivity, pipe diameter, and flow rate have a significant impact on thermal performance, with deratings varying from 0% to 64%. The cooling efficiency dropped from 18.7°C to 16.6°C for soil with a thermal conductivity of 0.52 W/m/K after 24 hours of continuous operation. An intense review of GCHE with their different design parameters was carried out by different authors. [1,3,4,5,6]. Taurines et al. [7] developed a three-dimensional numerical model and investigated the hygroscopic and complex behaviour of GCHE under real conditions. Agarwal et al. [8] conducted a literature review on the thermal performance of GCHE and reported that GCHE provides significant energy-saving equipment for both cooling and heating applications, with potential energy consumption reductions of 50%. The authors discussed various design parameters, such as burial depth, pipe diameter, soil conductivity, pipe layout, and different configurations. Florides and Kalogirou [9] also discussed the various applications of GCHEs, including residential and commercial buildings, industrial processes, and agriculture, and highlighted the potential energy savings and environmental benefits of GCHEs. Benzaama et al. [10] investigated the combined effect of GCHE and SSS using

experimental and Artificial Neural Networks (ANNs) models. They investigated the effect of temperature and humidity of air entering and leaving the GCHE, the temperature of the water in the SSS tank, and the power consumption of the heat pump. The ANN model predicted the temperature and humidity of the air leaving the GCHE with 90% accuracy. Lin et al. [11] employed the Taguchi method to optimize the efficiency of a building-coupled GCHE. The study focused on improving thermal performance based on parameters such as pipe length and diameter, insulation thickness, and structure aspect. The thermal performance of solar chimneys coupled with GCHE was investigated by Bai et al. [12]. The SCGCHE system effectively reduced indoor air temperature and relative humidity, and increased air velocity and CO_2 concentration removal rate. The maximum reduction in air temperature and relative humidity was found to be 4.7°C and 11.5% during summer whereas during the winter season, the highest temperature and humidity rise was found to be 3.4°C and 4.4%, respectively, while CO_2 concentration removal rate reached up to 70% to 74% in both seasons, respectively. Shahsavar et al. [13] investigated the energy, exergy, and economic analysis of building-integrated photovoltaic/thermal, GCHE, and hybrid systems. The integrated system provides increased energy and exergy efficiencies compared to individual systems due to the synergistic effects of combining different technologies. Misra et al. [14] evaluated the thermal performance and energy conservation potential of a hybrid air conditioning coupled with a GCHE. The conditioned air of GCHE was used for cooling the condenser coil of a 1.5 TR window air conditioning system and was found to reduce the power input by 16.11% compared to atmospheric air inlet conditions.

The ground-coupled heat exchangers (GCHEs) are energy-efficient and environment-friendly techniques that are used for building heating and cooling. GCHEs are especially helpful for reducing the cooling load on buildings in hot and dry seasons in the Indian climate conditions. Bansal et al. [15, 16] evaluated the performance of PVC and steel-piped GCHE systems for summer and winter conditioning. The temperature rises of 4.5°C and 4.8°C were found for the flow of 2 m/s of PVC and steel pipe, respectively, whereas temperature drops of 10.3 °C and 12.3 °C were seen for two different GCHEs. The performance was found to be independent of pipe materials. Bisoniya et al. [17, 18] estimated the heating and cooling potentials of GCHE for the winter and summer seasons of Bhopal, India. The numerical study was based on different parameters, such as flow conditions, pipe dimensions, and installation depths. The thermal efficiency of a GCHE system was found to be significantly influenced by the airflow rate. The temperature rises of 8.2 °C and 6.8 °C were observed for the airflow of 2 m/s and 5 m/s, respectively, whereas total heating potential was observed to be 0.59 MJ h to 1.22 MJ h. The temperature drops and cooling capacity was observed to be 12.9 °C to 11.30 °C and 0.85 MJ h to 1.87 MJ h, respectively, for the flow of 2 m/s to 5 m/s, respectively. The performance of a solar-air heater integrated with GCHE was studied by Soni et al. [19]. The introduction of the solar-air heating duct led to a heating capacity increase of 1217 kWh to 1280 kWh, whereas a temperature rises of 1.1°C-3.5°C was seen. Congedo et al. [20] conducted an experimental and numerical investigation of the GCHE coupled with a heat pump to assess the performance of the system in terms of heat transfer and energy efficiency. The performance of GCHE is influenced by different parameters, including the ground temperature, air velocity, and environmental conditions. A very impactful study with different operating parameters of GCHE was carried out by Agrawal et al. [21, 22, 23, 24]. The thermal conductivity, moisture content, and soil porosity are found to be important factors in the heat transfer analysis of the GCHE. The heat exchange capacity was also found to increase by 15.2% in the water-impregnated wet condition compared to the dry condition [22]. The efficiency of GCHE is found to be improved by adding sand-bentonite as a backfilling material. A more efficient heat transfer between the air inside the pipes and the surrounding soil was observed in this case [23]. The author, in a later study [24], investigated the economic feasibility of backfilling for the GCHE system. They studied heat transfer and pressure drop of GCHE using backfilling materials such as sand, bentonite, and a sand-bentonite mixture. They found that the sand-bentonite mixture exhibits high heat transfer characteristics, with a thermal resistance of 0.034 m^2- K/W and a pressure drop of 2.1 Pa/m. Singhal et al. [25] investigated the thermal performance of a GCHE coupled with a greenhouse and maintained a temperature of 25 °C to 35 °C for the growth of plants. The temperature of the greenhouse was found to be reduced by 4 °C below the atmospheric temperature and further reduced by 7 °C using

shading by a polyethene cover coupled with GCHEs. Kaushal [26] reported the performance of GCHE in the lower Himalayan region of India. The GCHE provides heating and cooling with an overall efficiency of 75%. The GCHE system has found a payback period of only 2-3 years, making it highly cost-effective for residential heating and cooling in the Lower Himalayan region. A unique GCHE with a plenum chamber was studied by Yang et al. [27]. A laboratory-scale GCHE system with an inlet plenum chamber, an underground pipe, and an outlet plenum chamber was used in this experiment. The input plenum chamber increased the thermal performance of the GCHE system in comparison to a traditional system, increasing the cooling capacity by 20%. Alkaragoly et al. [28] studied a hybrid GCHE comprising a photovoltaic solar chimney and a GCHE for enhancing thermal comfort in a building. The experiments were conducted with a small-scale prototype in a laboratory. The hybrid system showed a more comfortable indoor environment than the conventional ventilation. The indoor air temperature and humidity were maintained comfortably, and the cooling load was reduced by 48%. Yadav et al. [29] developed a semi-transparent photovoltaic greenhouse coupled with GCHE. The temperature range of 30 °C - 37 °C was maintained through ventilation and coupling with GCHE, making the system sustainable. Agrawal et al. [30] compared the thermal performance of a GCHE with U-shaped, helical and slinky layouts. The performance of GCHE is found to depend on the pipe layouts, temperature drop, and required power, whereas the heat transfer rate and temperature drop per unit length were observed to be higher for the slinky layout.

In this paper, the thermal performance of circular and rectangular cross-sectional GCHE with four different designs, horizontal, U-shaped, helical, and slinky, is numerically investigated using ANSYS Fluent solver. The simulation is carried out with a constant hydraulic diameter and length of 0.1016 m and 24.6 m, respectively.

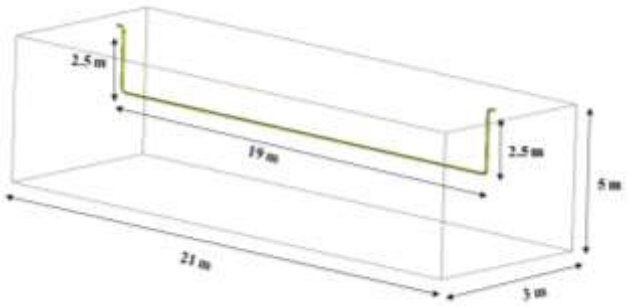
The main objectives of the present study are:

- To improve the design of GCHE to achieve higher cooling performance while meeting space constraints.
- To perform a simulation for the best suitable layout of GCHE for optimum performance and reduced installation space.
- To compare the thermal performance between circular and rectangular cross-sectional GCHE among all layouts.
- To examine the heat transfer and flow characteristics in different geometries of GCHE through temperature and pressure contours.
- To optimize the length of GCHE for different metrological temperatures in different conditions.
- To examine the variation of Nusselt number, Reynolds number, and pressure drop at different mass flow conditions at a fixed hydraulic diameter of 0.1016 m.

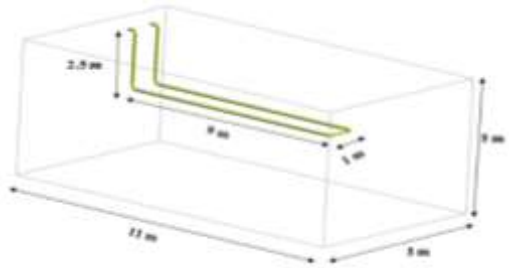
2. Methodology

2.1 Details of the CFD model

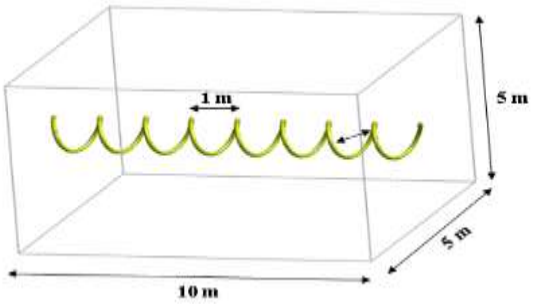
In this study, the performance of four different layouts, viz., horizontal, U-shape, helical, and slinky, with circular and rectangular cross-sections, is numerically analyzed for the fixed hydraulic diameter of 0.1016 m and length of 24.6 m. Figure 2 shows the GCHE, which is enclosed within a rectangular soil block with uniform temperature gradient of 300.2 K. The soil volumes of 21m ×3m×5 m, 11m ×3m×5m, 10m ×5m×5 m, and 10m ×3m×5 m are considered for corresponding layouts. The pitch diameter for helical and slinky layouts is considered to be 1 m. The sectional view of the circular and rectangular cross-sections of the GCHE layouts is also depicted in the same figure. The main purpose of the present study is to analyze the heat transfer and temperature reduction in each configuration of the GCHE.



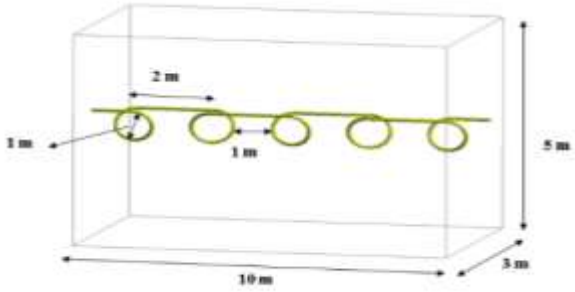
(a) Horizontal-shaped GCHE



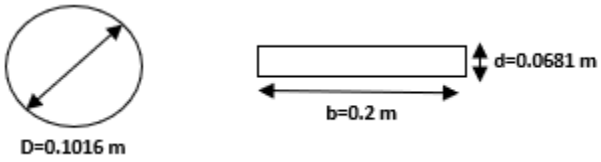
(b) U-shaped GCHE



(c) Helical-shaped GCHE



(d) Slinky-shaped GCHE



(e) Cross-sectional views of circular and rectangular sections

Figure 2. Schematic of horizontal, U-shaped, helical, and slinky layout GCHE.

The mesh of GCHE is generated using a 3-dimensional hybrid mesh system (hexa-dominant and tetrahedral) in ANSYS Fluent solver. The mesh elements' size ranges from 4.8 mm to 1.1 mm, with a growth rate of 1.24. Figure 3 shows the sectional view of a U-shaped GCHE with a circular cross-section.

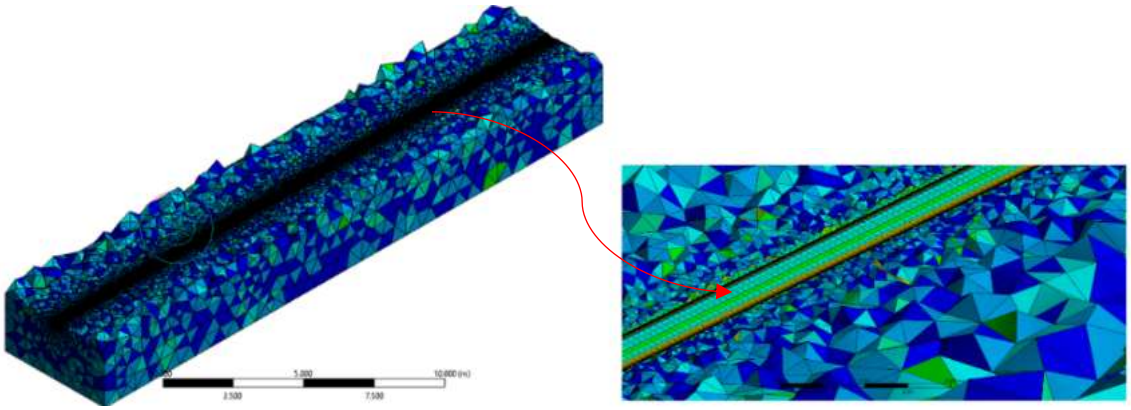


Figure 3. Cross-sectional view of the mesh generation for a circular cross-sectional GCHE.

2.2 Governing equations

Steady and incompressible flow assumptions are applied for the GCHE. The study employs the following governing equations.

Conservation of mass equation:

$$\nabla \cdot (\rho * V) = 0 \quad (1)$$

Conservation of momentum:

x-direction:

$$\rho * (V_x * \nabla) V_x = -\nabla P_x + \nabla \cdot \tau_x + \rho * g_x \quad (2a)$$

y-direction:

$$\rho * (V_y * \nabla) V_y = -\nabla P_y + \nabla \cdot \tau_y + \rho * g_y \quad (2b)$$

z-direction

$$\rho * (V_z * \nabla) V_z = -\nabla P_z + \nabla \cdot \tau_z + \rho * g_z \quad (2c)$$

Conservation of energy:

$$\rho * (V \cdot \nabla) h = \nabla \cdot (k * \nabla T) + Q \quad (3)$$

Where,

ρ is the density of air

V is the velocity vector ($V = V_x, V_y, V_z$),

P_x, P_y, P_z are the pressure components,

τ_x, τ_y, τ_z are the viscous shear stress,

g_x, g_y, g_z are the components of acceleration due to gravity,

h is the specific enthalpy of fluid,

k thermal conductivity of the fluid,

T is the temperature, and Q represents the heat source/sink term.

2.3 Boundary conditions

The x component of velocity (u= 1 m/s to 5 m/s) is specified at the inlet domain, while the Dirichlet boundary condition is applied for the two velocity components. The air temperature is set at 316.4 K, while 1 atmospheric pressure is specified at the outlet of the domain. The no-slip condition for velocity is applied at the pipe wall. To replicate heat transfer between the pipe wall and the ground, adequate thermal aspects have been assigned to the surrounding soil region. The solver employs the finite volume technique (FVM) to discretize the governing equations across the computational domain. The solution was considered convergent when the residuals attained 10^{-6} for the energy equation and 10^{-3} for continuity and velocity components, with measured variables exhibiting a consistent pattern.

Here are some assumptions used in the design of a GCHE:

- The GCHE is assumed to operate in a steady-state condition.
- The homogeneous and isotropic material is considered.
- The soil properties are assumed to be the same in all directions, and the heat exchanger pipe has perfect contact with the soil with negligible thermal resistance.
- Moisture condensation does not significantly affect the system's cooling capacity, and the air flowing through the tubes is uniform along its entire length.
- The PVC pipe used in the system is uniform in structure.

2.4 Description of Turbulence Model:

The present study uses a standard *k-ε* turbulent numerical model for simulation.

The transport equation for *k* (turbulent kinetic energy), in the context of the standard *k-ε* turbulent model, is given by:

$$\nabla \cdot (\rho U k) = \nabla \cdot \left[\left(\mu + \frac{\mu_t}{\sigma_k} \right) \cdot \nabla k \right] + P_k + P_b - \rho\varepsilon + S_k \qquad (4)$$

P_k and P_b are the generations of turbulent kinetic energy due to the mean velocity of shear and buoyancy effect, respectively. S_k is a user-defined source term.

The transport equation for ε (turbulent dissipation rate) is,

$$\nabla \cdot (\rho \varepsilon U) = \nabla \cdot \left[\left(\mu + \frac{\mu_t}{\sigma_\varepsilon} \right) \nabla \varepsilon \right] + C_1 \frac{\varepsilon}{k} (P_k + C_3 P_b) - C_2 \rho \frac{\varepsilon^2}{k} + S_\varepsilon \qquad (5)$$

The turbulent (or eddy) viscosity, $\mu_t = C_\mu \dfrac{\rho k^2}{\varepsilon}$

The coefficients C_1, C_2, and C_3 may vary between different models. The model constants C_1, C_2, C_μ, σ_k, and σ_ε have the following default values: C_1 =1.44, C_2 = 1.92, $C\mu$ = 0.09, σ_k =1.0, σ_ε = 1.3.

Table 1 Thermophysical details

Parameters(s)	**Materials**		
	Air	**Soil**	**PVC**
C_P	1005	1840.5	900.35
k	0.020	0.520	0.16
ρ	1.23	2051	1379

2.5 Grid-independent test and validation

In a CFD analysis, selecting the optimum mesh size is important for accurately simulating fluid flow and heat transfer problems. The grid-independence test is a typical approach to identifying the most appropriate mesh size for a given problem. The test was conducted for the circular U-shaped GCHE at an airflow of 2 m/s. The simulations were carried out using three different meshes of fine, medium, and coarse having respective grid sizes of 0.1 m, 0.15 m, and 0.2 m, respectively. The corresponding nodes and elements are mentioned in Table 2. The fine and medium meshes exhibit a slight temperature fluctuation after analysing the temperature profiles at each mesh, as shown in Figure 4. A mesh with a 0.15 m grid size is considered for further investigation.

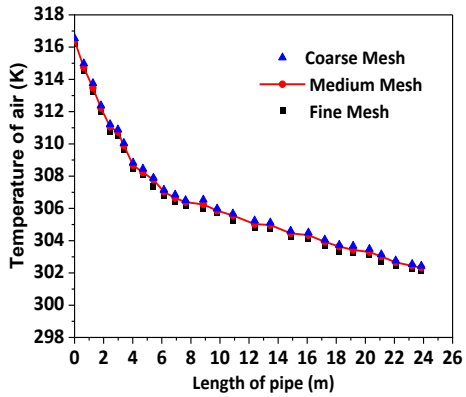


Figure 4. Temperatures at different sections for different meshes.

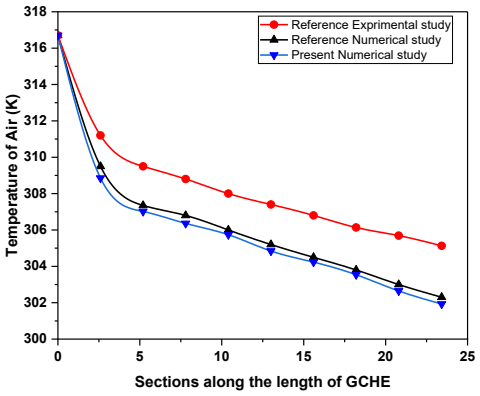


Figure 5 (a). Temperature at different sections of GCHE (Re =14210.4).

The numerical and experimental results of Bansal et al. [16] are used to validate the present numerical study. The simulations were carried out for circular configurations at a fixed Re = 13210.47 and Pr = 0.71. Figure 5 (a) shows the temperature profile at the different sections of the GCHE for both present and published results. The comparison between the simulation results and the published results shows a good agreement with a low value of the determination coefficient (R^2= 0.756 and Adjusted R^2 = 0.725). The error between the present numerical study and the experimental results occurred due to fluctuation of underground temperature, conduction heat loss, thermocouple sensitivity, etc. Figure 5 (b) represents the linear regression for the present study with a negative slope of 0.46, as air temperature decreases along the sections of GCHE.

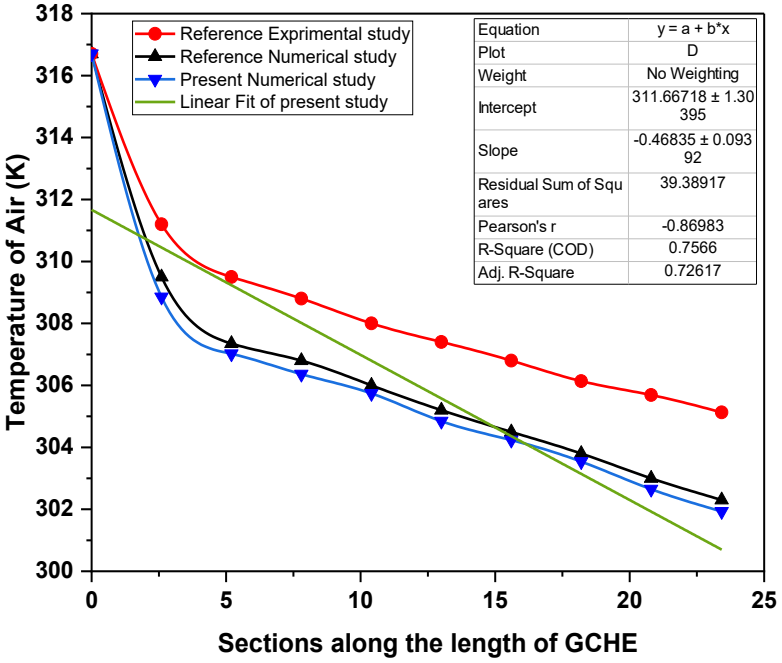


Figure 5 (b). Linear Regression of the present study.

Table 2 Mesh sizes used for grid independence test		
Mesh type	**No. of nodes**	**No. of elements**
Coarse	575897	986704
Medium	890932	1880762
Fine	1879436	4208759

2.6 Performance calculations of the GCHE system

There are two modes of heat transfer in the study of GCHE. Inside the pipe, heat transfer occurred due to convection between the flowing air and the inner wall, while conduction takes place due to the thickness of the pipe. On the other hand, the heat transfer between the outer wall and soil is primarily a conduction phenomenon. These distinctions in heat transfer mechanisms are important to consider while modelling and analysing the performance of GCHE.

Cooling capacity of the GCHE,

$$Q_c = \rho_a A_c v C_p (T_{ai} - T_{ao}) \quad (6)$$

The coefficient of performance (COP) of GCHE,

$$COP = \frac{Q_c}{Q_{in}} \quad (7)$$

The effectiveness of GCHE is the measure of the actual heat transfer relative to the maximum possible heat transfer and is evaluated from the following equation:

$$\mathrm{E} = \frac{\text{Actual heat transfer}}{\text{Maximum posssible heat transfer}} = \frac{\text{Actual temperature drop}}{\text{Maximum posssible temperature drop}}$$

$$\mathrm{E} = \frac{t_{ai} - t_{ao}}{t_{ai} - t_s} \quad (8)$$

Where, t_{ai} =inlet temperature, t_{ao}= outlet temperature and t_s =soil temperature

The coefficient of convection heat transfer (h_a) of air is calculated as follows,

$$h_a = \frac{N_u K_p}{D_h} \quad (9)$$

Here $N_u = f(R_e, P_r)$

For the laminar flow condition, the N_u is calculated as,

$N_u = 4.36$ Uniform heat flow

$N_u = 3.67$ Constant wall temperature

Under fully developed turbulent flow conditions, the Nusselt number is expressed as follows:

$$N_u = \frac{\left[f/8\right]\left[R_e - 1000\right]P_r}{1 + 12.7\left[f/8\right]^{0.5}\left[P_r^{2/3} - 1\right]} \quad (10)$$

For $0.5 < P_r < 2000$ and $2300 < R_e < 5\times10^6$

where 'f'indicates the friction factor.

Petukhov's relation applies to the friction factor in smooth pipe

$$f = (0.79 \ln R_e - 1.64)^{-2} \quad (11)$$

Pressure-drop, $\Delta P = \frac{f L v^2 \rho_a}{2 D_h}$ (12)

Energy consumption by the blower is calculated by

$$Q_{in} = \frac{(\Delta P)\rho A_c v}{\eta_{blower}} \quad (13)$$

For the present calculation, the blower efficiency is considered between the range of 0.6 and 0.7.

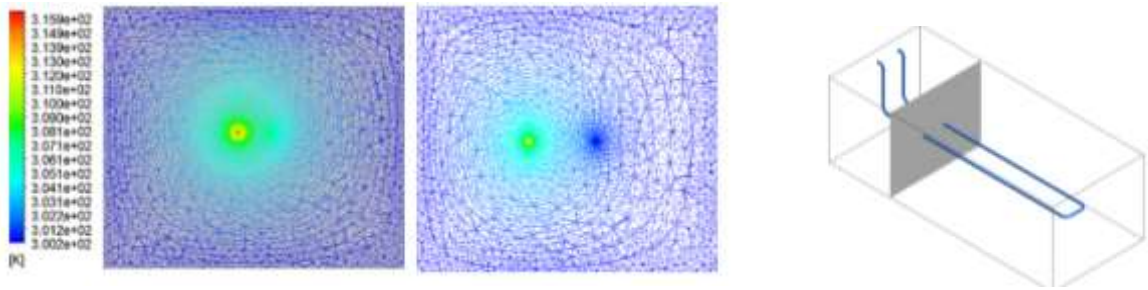
3. Result and Discussions

The main concern with installing any GCHE is limited space. The selection of the site is dependent on the environmental conditions, soil properties, and solar radiation of a particular location. So, the researchers are focused on the design and development of the GCHE for environmental sustainability in the heating, ventilation, and air conditioning of a building. The design of a GCHE is such that it can be installed in a very small space and requires minimal initial cost.

3.1 Effect of pipe spacing

The performance of GCHE is significantly affected by the spacing between pipes. The heat dissipation occurs in the radial direction, surrounding the wall of the GCHE. The pipes that are too close together restrict the heat transfer in the radial direction of the surrounding soils and reduce the heat transfer. Therefore, the spacing between pipes should be adjusted to optimize the performance of the GCHE.

In this study, the U-shaped GCHE with pipe spacing of 0.5 m, 1 m, and 1.5 m is numerically simulated using ANSYS. The temperature contour for 0.5 m and 1 m pipe spacing is presented in Figure 6. In the case of GCHE with a pipe spacing of 0.5 m, the heat-transferring zones overlap, reducing the heat dissipation rate to the surrounding soil. In contrast, a 1 m spacing yields a uniform temperature distribution with minimal thermal overlap, resulting in stable temperature gradients and improved heat-transfer effectiveness. Although 1.5 m spacing offers the least interference, it requires more land, making 1 m an acceptable compromise between performance and space requirements. The soil around the 1 m configuration recovers temperature more quickly, reduces thermal saturation, and yields a better outlet air temperature. Therefore, for space-constrained applications, a GCHE with 1 m pipe spacing is selected for further analysis. In the present study, the distance between two adjacent pipes is taken as 1 m for a U-shaped layout, and the pitch diameter of helical and slinky layouts is also considered as 1 m.

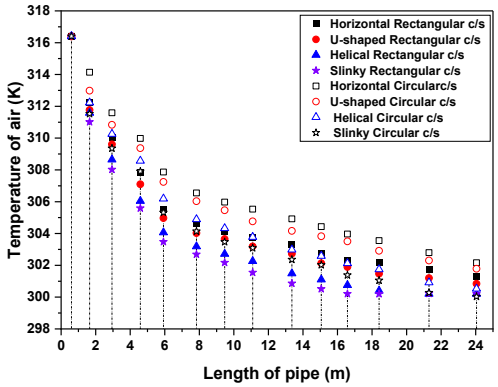


(a) (b) (c)

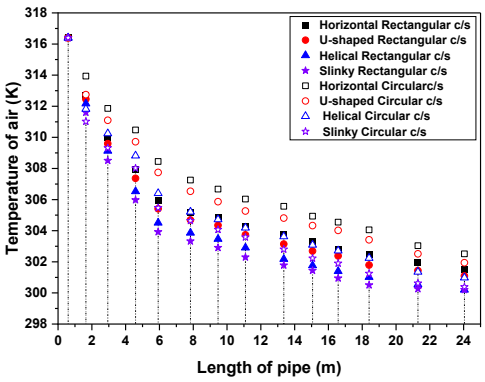
Figure 6. Temperature contour at a fixed location for the U-shaped GCHE for the canter space of (a) 0.5 m and (b) 1 m

3.2 Effect of the cross-sectional area

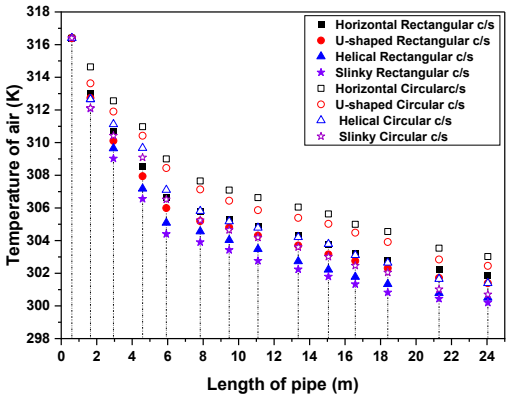
The performance of rectangular and circular cross-sections with fixed hydraulic diameter D_h = 0.1016 m is studied for different layouts, viz., horizontal, U-shape, helical, and slinky-shaped. The cross-sectional area of rectangular GCHE is larger than that of circular GCHE with the same hydraulic diameter. The air temperature at different sections for all the layouts at three different velocities, 2 m/s, 3 m/s and 5 m/s, is shown in Figure 7. The optimal temperature of 300.2 K is reached at a shorter distance for all configurations in the case of a rectangular GCHE compared to a circular GCHE at all air velocities. The temperature at the exit section of a circular cross-section with a fixed air velocity of 2 m/s for the simple horizontal, U-shaped, helical and slinky layout is found to be 302.159 K, 301.586 K, 300.647 K and 300.20 K respectively, whereas the same temperatures are achieved in rectangular cross-section GCHE at a length of 18.82 m, 17.46 m, 16.09 m, and 15.43 m respectively. The surrounding soil of the rectangular cross-section exhibits a short temperature disturbance range and shows more consistency with the wall temperature. The GCHE with a rectangular cross-section shows a greater reduction in temperature across all sections, as shown in Figure 8. The rectangular cross-section with a slinky design shows the greatest temperature reduction along its length. In this case, the contact area of the soil and the GCHE is larger and allows better conduction between the pipe wall and the soil. The temperature of the wall remains more consistent and provides more efficient cooling in this case. The air temperature variation along the length of a rectangular GCHE becomes relatively small beyond a certain length, while in the case of a circular cross-section, the temperature decreases throughout the sections until it reaches a limiting length.



(a) V= 2 m/s



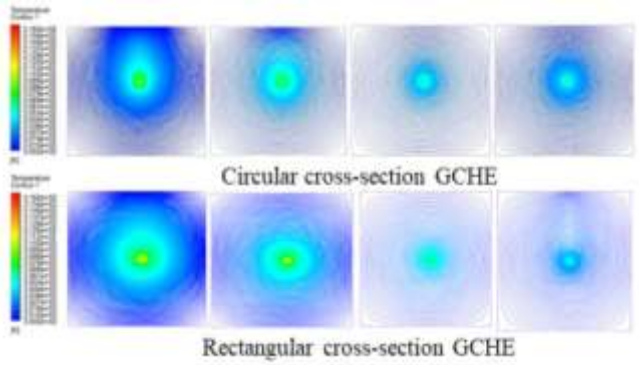
(b) V= 3 m/s



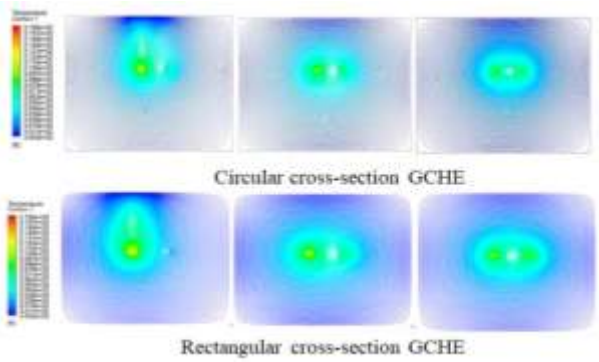
(b) V= 5 m/s

Figure 7. Effect of cross-sectional areas for the horizontal, U-shaped, helical, and slinky layouts at a fixed velocity of 2 m/s, 3m/s, and 5 m/s.

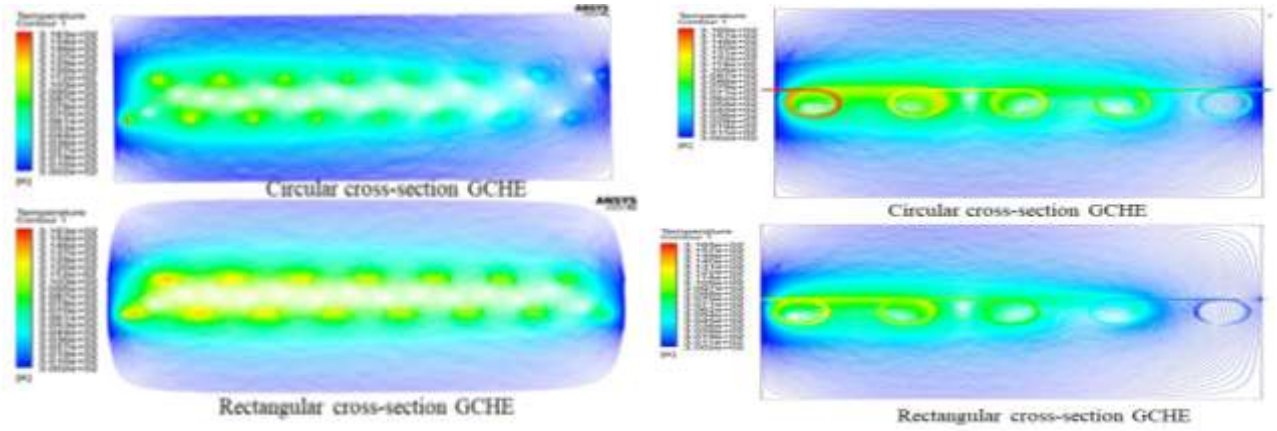
The temperature contours of the horizontal, u-shaped, helical, and slinky GCHE at a flow rate of 2 m/s are shown in Figure 8. The rectangular cross-sections show more uniform temperature distribution compared to circular ones, while the slinky layouts with rectangular cross-sections exhibit the most significant temperature drop and are found to enhance cooling efficiency. The temperature of the soil that surrounds the outer wall of the GCHE is found to be reduced and reaches the ground's undisturbed temperature.



(a) Horizontal layout



(b) U-shaped layout

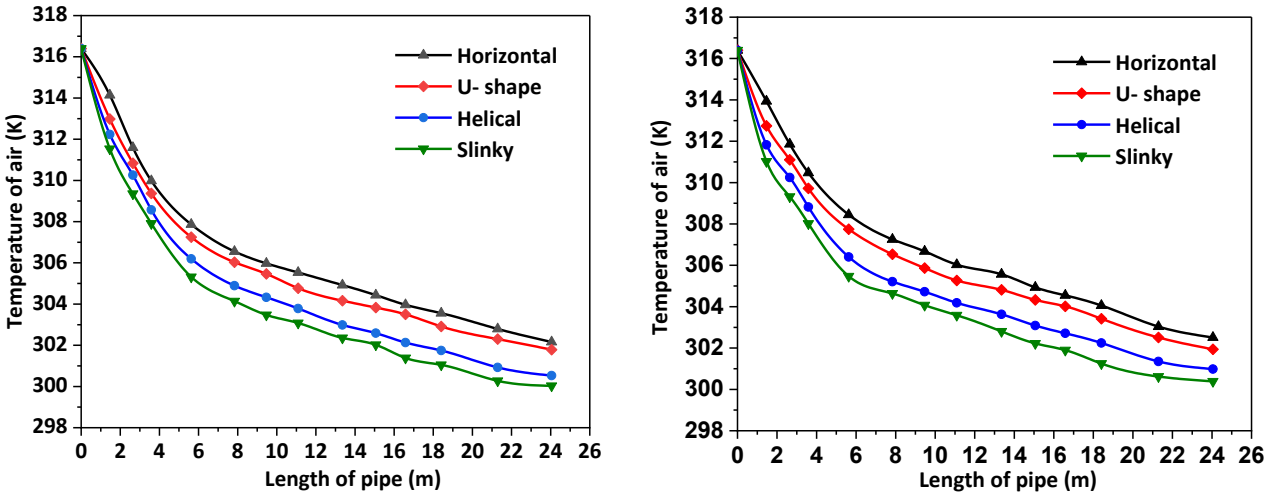


(c) Helical layout (d) Slinky layout

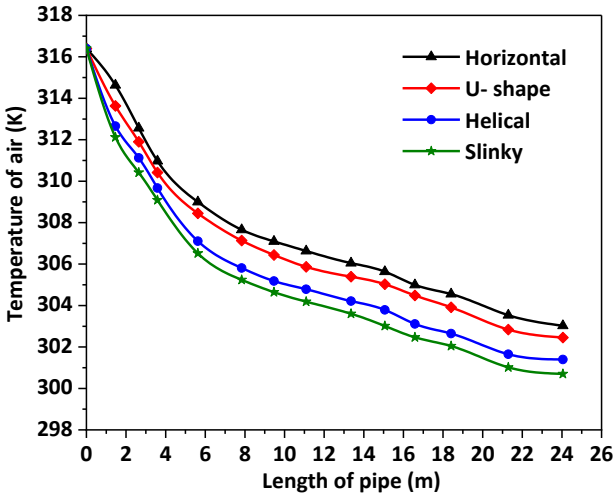
Figure 8. Temperature contour of circular and rectangular GCHE for the horizontal, u-shaped, helical, and slinky layout.

3.3 Effect of layouts

The performance of rectangular and circular cross-sectional GCHEs for different layouts is examined in this section. The temperature drops along the length at different air velocities for individual layouts are shown in Figures 9 and 10.



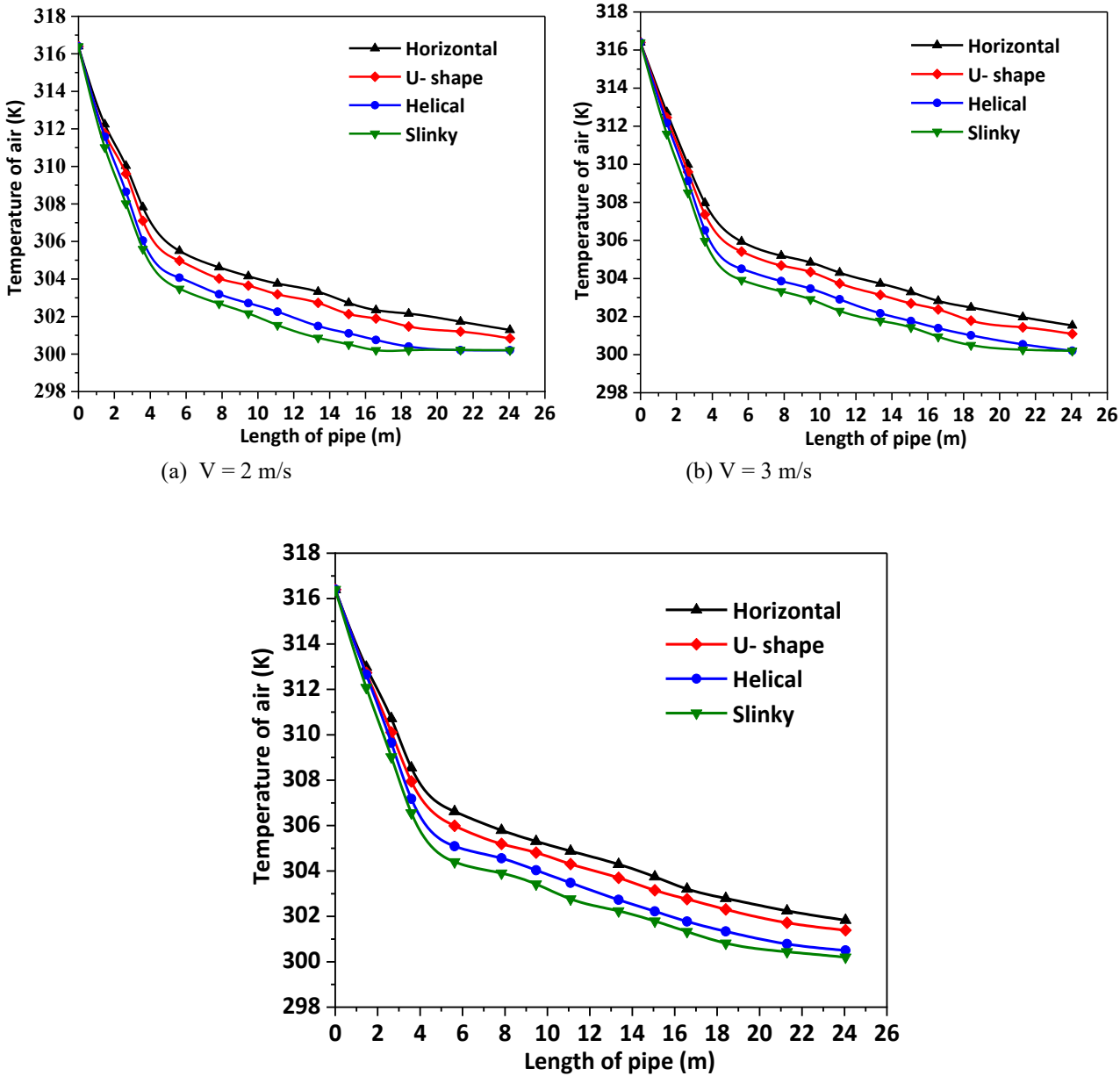
(a) V= 2 m/s (b) V= 3 m/s



(c) V= 5 m/s

Figure 9. Effect of different layouts for circular cross-sectional GCHE at (a) 2 m/s, (b) 3 m/s, and (c) 5 m/s.

The slinky layout shows the higher temperature drop followed by helical and U-shape compared to the horizontal layout GCHE for all velocities of 2, 3, and 5 m/s in both circular and rectangular cross-section GCHE. Figure 9 shows the temperature drop along the different sections of GCHE at velocities of 2, 3, and 5 m/s for the circular cross-section. The optimum temperature of 300.2 K is obtained at a section of 21.3 m from the inlet in the case of a slinky layout, while the temperature of 303.46 K, 302.82 K, and 300.74 K is observed for horizontal, U-shaped, and helical GCHE, respectively, at a fixed airflow of 2 m/s. The length of the circular cross-sectional GCHE having a slinky layout is found to be reduced by 17%, 13%, and 6% compared to the horizontal, U-shaped, and helical layouts.



(a) V = 2 m/s

(b) V = 3 m/s

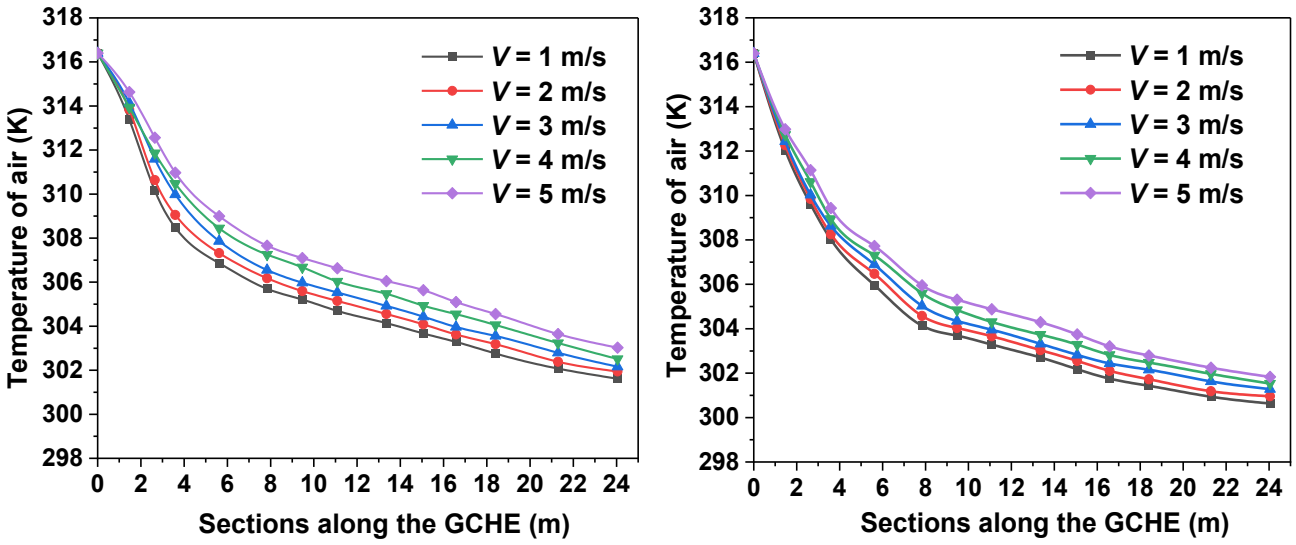
(c) V= 5 m/s

Figure 10. Effect of different layouts for rectangular cross-sectional GCHE at (a) 2 m/s, (b) 3 m/s, and (c) 5 m/s.

Figure 10 shows the temperature drop along the different sections of GCHE at velocities of 2, 3, and 5 m/s for the rectangular cross-section. For the GCHE with a rectangular cross-section, the optimal temperature of 300.2 K is reached at a section of 16.57 m and 19.73 m, respectively, at a fixed flow rate of 2 m/s. In contrast, when examining the horizontal and U-shaped layout GCHE, the temperature at the exit sections is found to be 301.28 K and 300.83 K, respectively. The reduction of length in the case of rectangular cross-sectional GCHE with the slinky layout is found to be 23%, 19%, and 8% with the other three respective layouts.

3.4 Effect of airflow

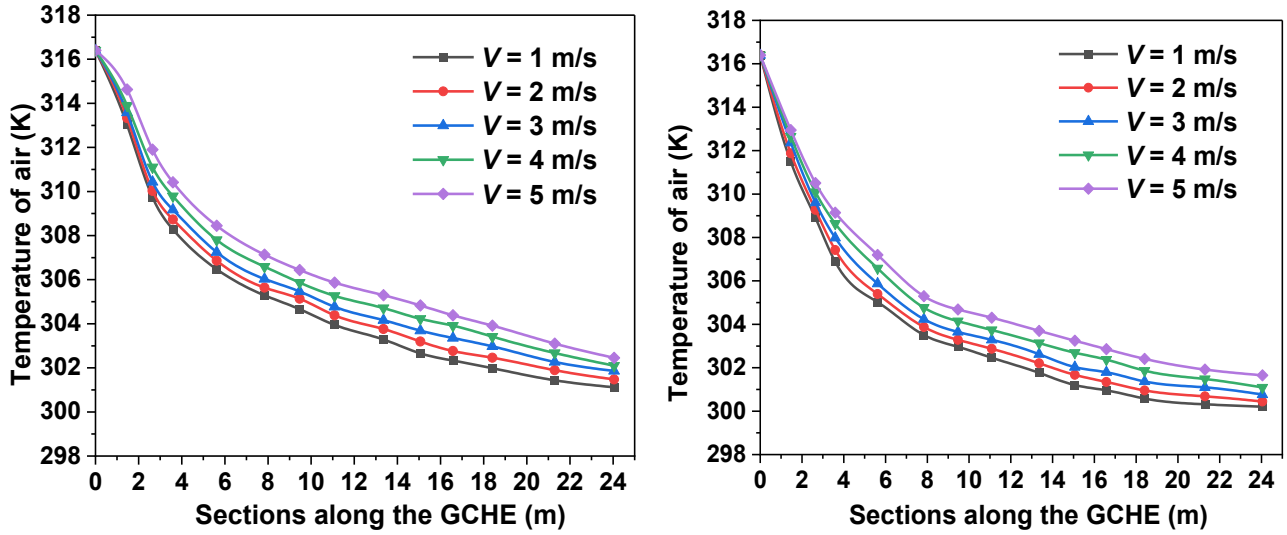
Air velocity significantly impacts the performance of GCHE and is a critical factor in heat transfer and energy consumption in the design of heat exchangers. The convection heat transfer is more dominant inside the GCHE. The temperature of flowing air inside the GCHE is found to be highly dependent on flow rate and more compatible with lower air velocity. The temperature drops at the different sections for horizontal, U-shaped, helical, and slinky layouts along the length at a velocity ranging from 1 m/s to 5 m/s for the circular and rectangular cross-sections, as shown in Figures 11, 12, 13, and 14, respectively.



(a) Circular cross-sectional GCHE (b) Rectangular cross-sectional GCHE

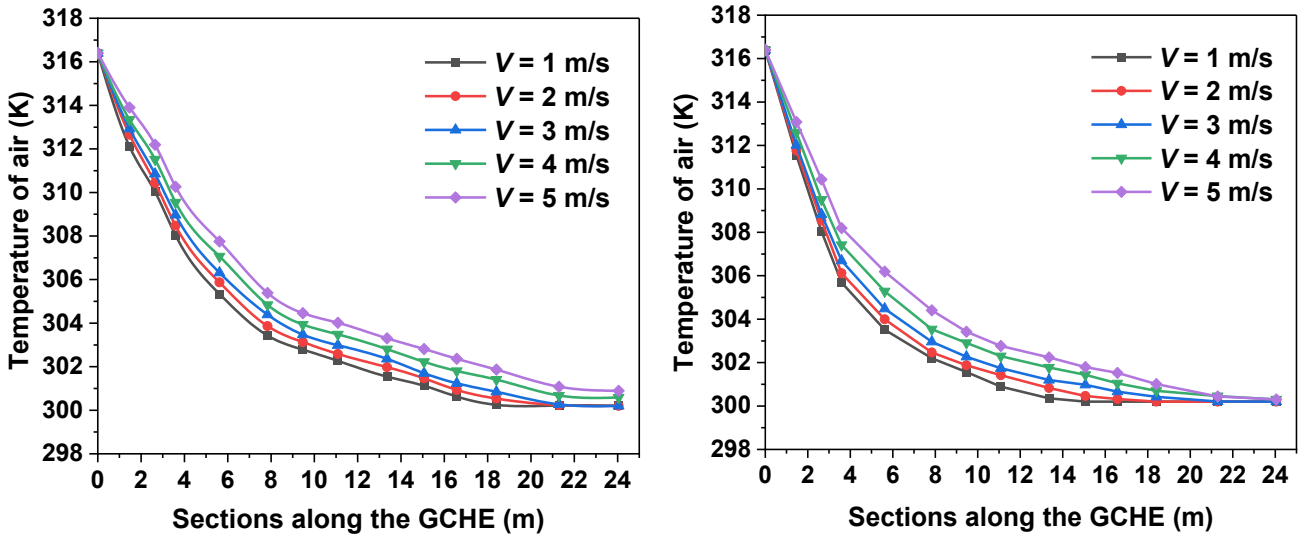
Figure 11. Temperature distribution at different sections of the horizontal layout GCHE.

The present study shows that increasing the airflow reduces the temperature drop for all layouts, with the maximum decrease occurring at the lowest airflow of 1 m/s in all the layouts. It has been seen that the temperature drop is reduced by 2.68 K – 1.37 K in the case of horizontal, U-shaped, helical and slinky layouts with circular cross-section GCHE as air velocity increases from 1 m/s to 5 m/s. Under similar operating conditions, the temperature drop in rectangular cross-section GCHE decreases by 1.32 K – 0.23 K for the respective layouts. As the air velocity increases, mass flow increases and increases the cooling capacity, which increases the thermal performance. When the air flow inside the GCHE decreases, it allows more time for convection heat transfer and decreases the air temperature across the sections. As the flow rate decreases, the temperature drop is observed to be higher for all the layouts. In addition, increasing airflow also increases the pressure drop across the GCHE, which increases energy consumption. The optimum temperature is observed at a short distance for the lower air flow condition for all the layouts, and the length of GCHE is reduced by 6% - 19% as air flow decreases from 5 m/s - 1 m/s. The air velocity has significant effects on the thermal performance, energy consumption, and comfort of the occupants.



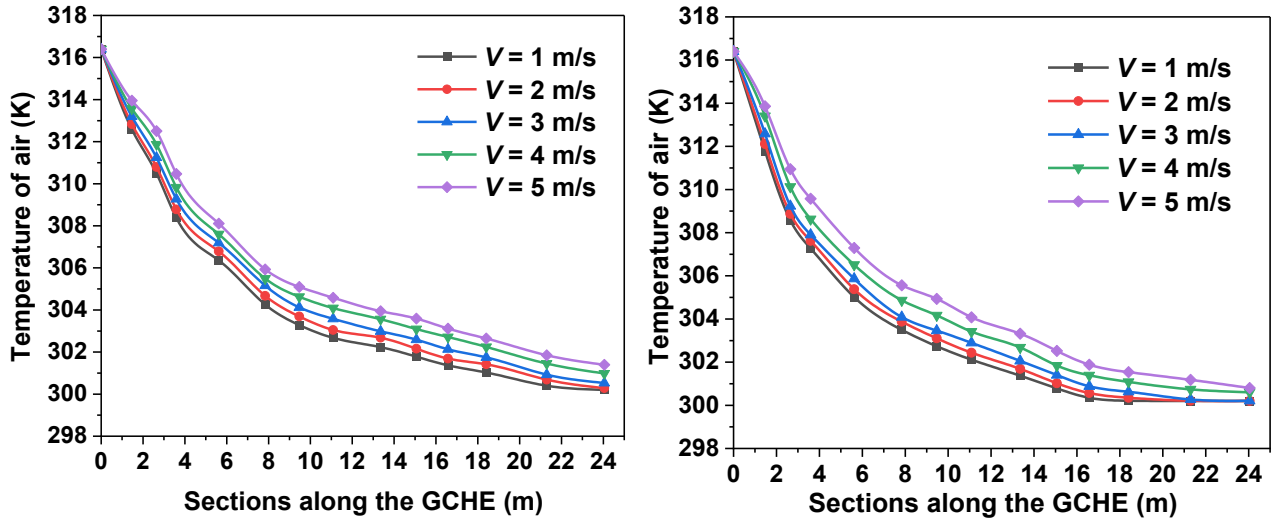
(a) Circular cross-sectional GCHE (b) Rectangular cross-sectional GCHE

Figure 12. Temperature distribution at different sections of the U-shaped layout GCHE.



(a) Circular cross-sectional (b) Rectangular cross-sectional GCHE

Figure 13. Temperature distribution at different sections of the slinky layout GCHE.



(a) Circular cross-sectional (b) Rectangular cross-sectional GCHE

Figure 14. Temperature distribution at different sections of the helical layout GCHE.

3.5 Effect of inlet air temperature

The temperature variation at the inlet of a GCHE has a substantial effect on its performance and efficiency. The inlet air temperature is relatively high during summer and hot climates, and GCHE provides more cooling effect due to a greater temperature difference. The underground temperature is usually cooler than the outdoor air, extracting more heat from the warm incoming air and releasing it into the soil before being supplied to the building. The inlet temperatures 316.4 K, 319 K, 321 K and 323 K are considered in this study for cooling conditions of both rectangular and circular cross-sectional GCHE, as shown in Figure 15. The net temperature difference is found to be higher in the case of rectangular cross-section GCHE in all layouts. It is also found that the slinky design gives the maximum temperature drop among all layouts. The optimum temperature of 300.2 K is achieved in this case only. As the inlet temperature increases from 316.4 K to 323 K, the outlet temperature is found to increase by 4.7 K, 4.3 K, 3.86 K, and 3.12 K, respectively, in the case of horizontal, U-shaped, helical and slinky layouts with circular cross-section. The outlet temperature is found to increase by 3.57 K, 3.15 K, 1.16 K, and 0 K in the corresponding layout with rectangular cross-section GCHEs. The temperature difference between the incoming air and the surrounding soil influences the overall performance of the GCHE. The maximum temperature difference leads to higher heat transfer rates and improved energy efficiency of the GCHE. The slinky design should consider the local climatic conditions, including seasonal temperature variations that meet the cooling demands of the building.

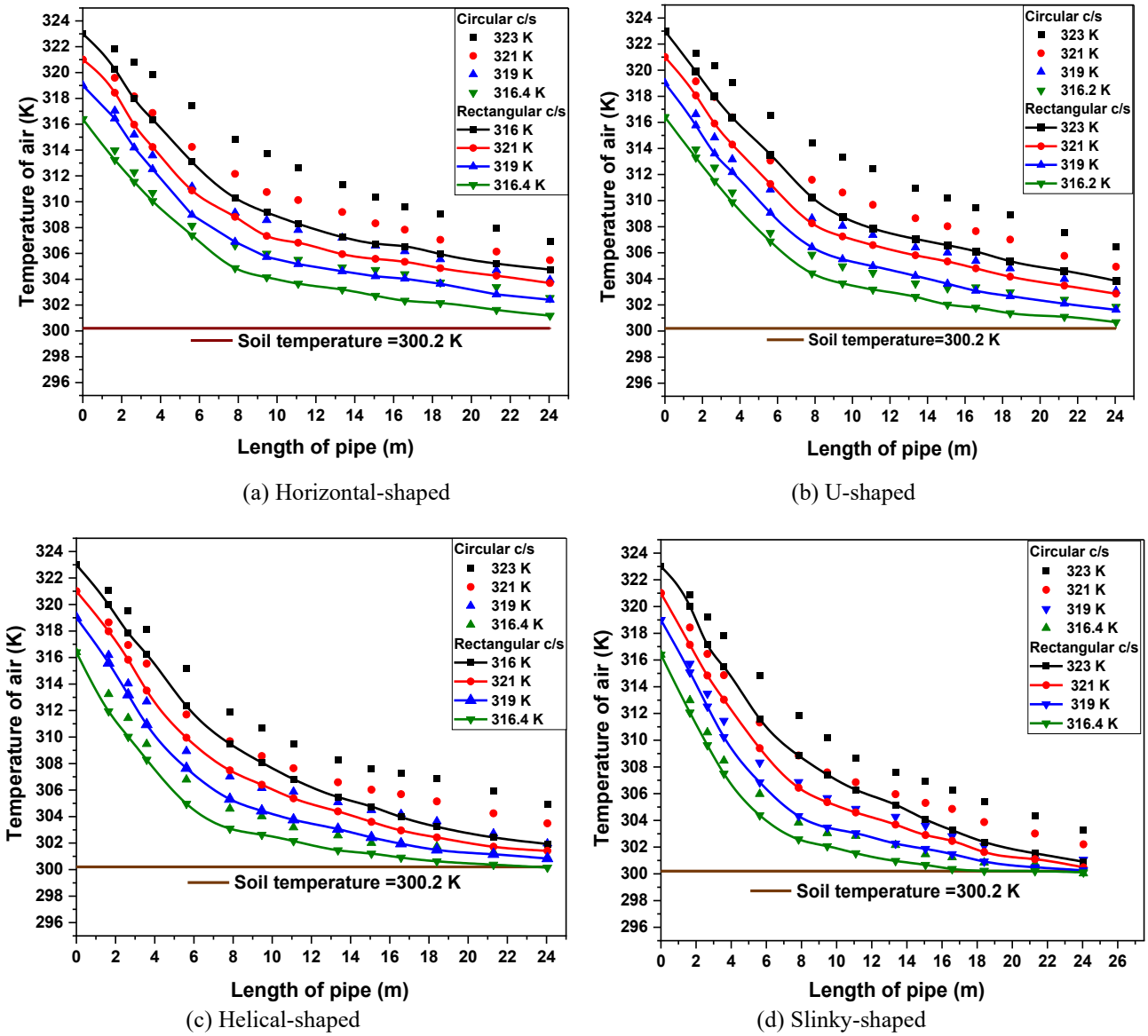
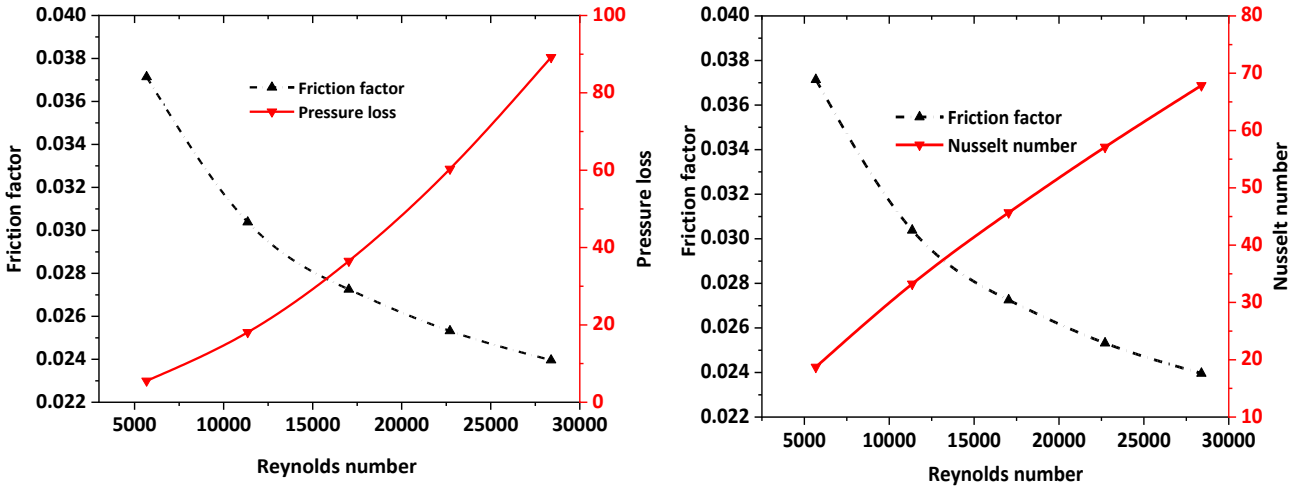


Figure 15. Temperature distribution for the different inlet air temperatures of horizontal, U-shaped, helical, and slinky layouts GCHE.

3.6 Variation of Nusselt number with Reynolds number and friction factor

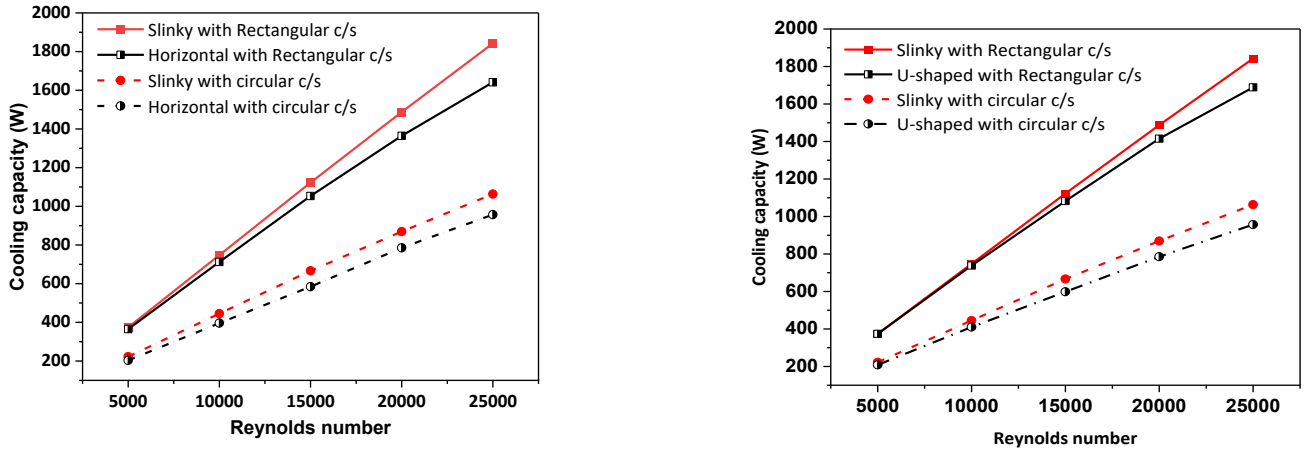
Nusselt number and friction factors are evaluated analytically using different correlations. Figure 16 illustrates the changes in the Nusselt number, friction factor, and pressure drop as functions of the Reynolds number. The friction factor decreases with an increase in the Reynolds number, due to an increase in the flow rate inside the pipe, while the pressure drop increases with the increase in the Reynolds number. As the Reynolds number increases from 5000 to 30000, the friction factor decreases from 0.037 to 0.023, indicating decreasing resistance to flow at higher velocity. In contrast, pressure loss exhibits a significantly increasing pattern, increasing from 5.83 at Re = 5000 to 90 at Re =30,000. As the Reynolds number increases, the flow becomes more turbulent; hence, the convective heat transfer rate increases.



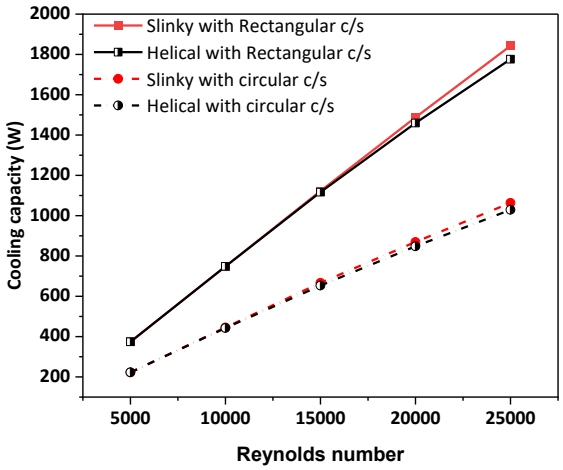
(a) (b)

Figure 16. Variation of Nusselt number, friction factor, and pressure loss at different Reynolds numbers.

The cooling capacity for the different flow rates and Reynolds numbers is shown in Figure 17. The cooling capacity of the GCHE depends on the temperature difference and the mass flow rate of air. A comparative study is carried out for horizontal, U-shaped, and helical layouts with the slinky layout for both circular and rectangular cross-sections of GCHEs. In all layouts, the rectangular GCHE exhibits the maximum temperature drop and maximum mass flow rate, while the slinky layout with a rectangular cross-section shows the highest cooling rates. The rectangular GCHE with slinky layout has a maximum cooling capacity of about 1842.47 W at Re ≈ 25000, whereas the horizontally shaped GCHE with circular layout has a minimum of about 202.86 W at Re ≈ 5000. The rectangular cross-sections offer 19.8 – 40.34% higher cooling capacity as compared to circular cross-sections over the different Reynolds number range.



(a) Slinky and horizontal GCHE (b) Slinky and U-shaped GCHE



(c) Slinky and helical GCHE

Figure 17. Comparison of the cooling capacity of slinky layout GCHE with horizontal, U-shaped, and helical GCHE.

4. Conclusions

In this study, the thermal performance of circular and rectangular GCHE of four different shapes, horizontal, U-shaped, helical, and slinky layouts are numerically analysed. The major findings of this study are as follows-

- The distance between the adjacent pipes is considered in such a way that the heat dissipation through the pipe to the ground takes place without any obstruction. The distance between the adjacent pipes must be 1 m so that the heat transfer in the radial direction is not disturbed.
- The slinky pipe layout shows the maximum temperature drop. The optimum temperature of 300.2 K is obtained at a shorter length in the slinky layout compared to other layouts.
- The thermal performance of the GCHE is also found to be dependent on the cross-sectional areas, and maximum performance is observed in the case of the slinky layout with a rectangular cross-section.
- The thermal performance is more dominant towards free convection heat transfer and mass flow rate, and optimal performance is achieved at lower airflow, although reducing air velocity decreases the cooling capacity of the GCHE.
- Increasing the inlet air temperature increases the net temperature difference, and the maximum rate of cooling is reported in the slinky layout.
- The friction factor is found to decrease with an increase in the Reynolds number, while the pressure drop increases with an increase in the Reynolds number.
- The cooling capacity is found to increase with Reynolds number, and optimum cooling capacity is observed for a rectangular with a slinky layout.

Data Availability Statement: "The data that support the findings of this study are available from the corresponding author upon reasonable request".

Disclosure of Interest: "No potential competing interest was reported by the authors."

Funding: "No funding was received."

References:

1. Bisoniya, Trilok Singh, Anil Kumar, and Prashant Baredar. "Experimental and analytical studies of earth–air heat exchanger (EAHE) systems in India: a review." Renewable and Sustainable Energy Reviews 19 (2013): 238-246.
2. Misra, Rohit, Vikas Bansal, Ghanshyam Das Agrawal, Jyotirmay Mathur, and Tarun K. Aseri. "CFD analysis based parametric study of derating factor for Earth Air Tunnel Heat Exchanger." Applied Energy 103 (2013): 266-277.

3. Florides, Georgios, and Soteris Kalogirou. "Ground heat exchangers—A review of systems, models and applications." Renewable energy 32, no. 15 (2007): 2461-2478.
4. Agrawal, Kamal Kumar, Ghanshyam Das Agrawal, Rohit Misra, Mayank Bhardwaj, and Doraj Kamal Jamuwa. "A review on effect of geometrical, flow and soil properties on the performance of Earth air tunnel heat exchanger." Energy and Buildings 176 (2018): 120-138.
5. Bansal, N. K., M. S. Sodha, and S. S. Bharadwaj. "Performance of earth air tunnels." International Journal of Energy Research 7, no. 4 (1983): 333-345.
6. Bharadwaj, S. S., and N. K. Bansal. "Temperature distribution inside ground for various surface conditions." Building and Environment 16, no. 3 (1981): 183-192.
7. Taurines, Kevin, Stéphanie Giroux-Julien, Mohammed Farid, and Christophe Ménézo. "Numerical modelling of a building integrated earth-to-air heat exchanger." Applied Energy 296 (2021): 117030.
8. Agrawal, Kamal Kumar, Rohit Misra, Ghanshyam Das Agrawal, Mayank Bhardwaj, and Doraj Kamal Jamuwa. "The state of art on the applications, technology integration, and latest research trends of earth-air-heat exchanger system." Geothermics 82 (2019): 34-50.
9. Florides, Georgios, and Soteris Kalogirou. "Ground heat exchangers—A review of systems, models and applications." Renewable energy 32, no. 15 (2007): 2461-2478.
10. Benzaama, M. H., S. Menhoudj, A. M. Mokhtari, and M. Lachi. "Comparative study of the thermal performance of an earth air heat exchanger and seasonal storage systems: Experimental validation of Artificial Neural Networks model." Journal of Energy Storage 53 (2022): 105177.
11. Lin, Yaolin, Haoming Feng, Wei Yang, Xiaoli Hao, Lin Tian, and Xingping Yuan. "Thermal performance optimization of a semi-nested building coupled with an earth-to-air heat exchanger using iterative Taguchi method." Renewable Energy 195 (2022): 1275-1290.
12. Bai, Yufu, Tianhe Long, Wuyan Li, Yongcai Li, Shuli Liu, Zhihao Wang, Jun Lu, and Sheng Huang. "Experimental investigation of natural ventilation characteristics of a solar chimney coupled with earth-air heat exchanger (SCEAHE) system in summer and winter." Renewable Energy 193 (2022): 1001-1018.
13. Shahsavar, Amin, Pouyan Talebizadehsardari, and Müslüm Arıcı. "Comparative energy, exergy, environmental, exergoeconomic, and enviroeconomic analysis of building integrated photovoltaic/thermal, earth-air heat exchanger, and hybrid systems." Journal of cleaner production 362 (2022): 132510.
14. Misra, Rohit, Vikas Bansal, Ghanshyam Das Agarwal, Jyotirmay Mathur, and Tarun Aseri. "Evaluating thermal performance and energy conservation potential of hybrid earth air tunnel heat exchanger in hot and dry climate—in situ measurement." Journal of Thermal Science and Engineering Applications 5, no. 3 (2013): 031006.
15. Bansal, Vikas, Rohit Misra, Ghanshyam Das Agrawal, and Jyotirmay Mathur. "Performance analysis of earth–pipe–air heat exchanger for winter heating." Energy and Buildings 41, no. 11 (2009): 1151-1154.
16. Bansal, Vikas, Rohit Misra, Ghanshyam Das Agrawal, and Jyotirmay Mathur. "Performance analysis of earth–pipe–air heat exchanger for summer cooling." Energy and buildings 42, no. 5 (2010): 645-648.
17. Bisoniya, Trilok Singh, Anil Kumar, and Prashant Baredar. “Cooling potential evaluation of earth-air heat exchanger system for summer season.” Int J Eng Tech Res 2(4), (2014):309-316.
18. Bisoniya, Trilok Singh, Anil Kumar, and Prashant Baredar. "Heating potential evaluation of earth–air heat exchanger system for winter season." Journal of Building Physics 39, no. 3 (2015): 242-260.
19. Soni, Manoj Kumar. "Thermal performance investigation of earth air tunnel heat exchanger coupled with a solar air heating duct for northwestern India." (2015).
20. Congedo, Paolo Maria, Cristina Baglivo, Sara Bonuso, and Delia D’Agostino. "Numerical and experimental analysis of the energy performance of an air-source heat pump (ASHP) coupled with a horizontal earth-to-air heat exchanger

(EAHX) in different climates." Geothermics 87 (2020): 101845.

21. Agrawal, Kamal Kumar, Ghanshyam Das Agrawal, Rohit Misra, Mayank Bhardwaj, and Doraj Kamal Jamuwa. "A review on effect of geometrical, flow and soil properties on the performance of Earth air tunnel heat exchanger." Energy and Buildings 176 (2018): 120-138.
22. Agrawal, Kamal Kumar, Rohit Misra, Tejpal Yadav, Ghanshyam Das Agrawal, and Doraj Kamal Jamuwa. "Experimental study to investigate the effect of water impregnation on thermal performance of earth air tunnel heat exchanger for summer cooling in hot and arid climate." Renewable energy 120 (2018): 255-265.
23. Agrawal, Kamal Kumar, Rohit Misra, and Ghanshyam Das Agrawal. "Improving the thermal performance of ground air heat exchanger system using sand-bentonite (in dry and wet condition) as backfilling material." Renewable Energy 146 (2020): 2008-2023.
24. Agrawal, Kamal Kumar, Rohit Misra, and Ghanshyam Das Agrawal. "CFD simulation study to evaluate the economic feasibility of backfilling materials for ground-air heat exchanger system." Geothermics 90 (2021): 102002.
25. Singhal, Samar, Ashwini Kumar Yadav, and Ravi Prakash. "An investigation of the thermal performance of a tropical greenhouse constructed with an earth air heat exchanger." Journal of Thermal Science and Engineering Applications 15, no. 11 (2023): 111013.
26. Kaushal, Maneesh. "Performance analysis of clean energy using geothermal earth to air heat exchanger (GEAHE) in Lower Himalayan Region–Case study scenario." Energy and Buildings 248 (2021): 111166.
27. Yang, Qizhi, Zhiru Hu, Yao Tao, Long Shi, Jiyuan Tu, Jie Chai, and Yong Wang. "Experimental and numerical study on cooling performance of a novel earth-to-air heat exchanger system with an inlet plenum chamber." Energy Conversion and Management 277 (2023): 116671.Qi, D., Li, S., Zhao, C., Xie, W., & Li, A. (2022). Structural optimization of multi-pipe earth to air heat exchanger in greenhouse. Geothermics, 98, 102288.
28. Alkaragoly, Mohammed, Mehdi Maerefat, Mohammed Zabetian Targhi, and Asmaa Abdljalel. "An innovative hybrid system consists of a photovoltaic solar chimney and an earth-air heat exchanger for thermal comfort in buildings." Case Studies in Thermal Engineering 40 (2022): 102546.
29. Yadav, Somil, Sarat Kumar Panda, G. N. Tiwari, Ibrahim M. Al-Helal, Abdullah A. Alsadon, Mohammed R. Shady, and Arvind Tiwari. "Semi-transparent photovoltaic thermal greenhouse system combined with earth air heat exchanger for hot climatic condition." Journal of Thermal Science and Engineering Applications 14, no. 8 (2022): 081007.
30. Agrawal, Kamal Kumar, Rohit Misra, Mayank Bhardwaj, Ghanshyam Das Agrawal, and Anuj Mathur. "Computational fluid dynamics simulation based comparison of different pipe layouts in an EATHE system for cooling operation." Journal of Thermal Science and Engineering Applications 11, no. 5 (2019): 051012.